

# Label-Free Imaging of Nanoparticle Uptake Competition in Single Cells by Hyperspectral Stimulated Raman Scattering

Bin Huang, Shuai Yan, Lin Xiao, Rong Ji, Liuyan Yang, Ai-Jun Miao,\* and Ping Wang\*

Imaging and quantification of nanoparticles in single cells in their most natural condition are expected to facilitate the biotechnological applications of nanoparticles and allow for better assessment of their biosafety risks. However, current imaging modalities either require tedious sample preparation or only apply to nanoparticles with specific physicochemical characteristics. Here, the emerging hyperspectral stimulated Raman scattering (SRS) microscopy, as a label-free and nondestructive imaging method, is used for the first time to investigate the subcellular distribution of nanoparticles in the protozoan *Tetrahymena thermophila*. The two frequently studied nanoparticles, polyacrylate-coated  $\alpha$ -Fe<sub>2</sub>O<sub>3</sub> and TiO<sub>2</sub>, are found to have different subcellular distribution pattern as a result of their dissimilar uptake routes. Significant uptake competition between these two types of nanoparticles is further discovered, which should be paid attention to in future bioapplications of nanoparticles. Overall, this study illustrates the great promise of hyperspectral SRS as an analytical imaging tool in nanobiotechnology and nanotoxicology.

## 1. Introduction

Nanoparticles (NPs) are particles <100 nm in at least two dimensions.<sup>[1]</sup> With recent advancements in nanobiotechnology, NPs have been evaluated in a wide range of life-science and medical applications. To meet the demands of these and other applications, huge amounts of NPs are being produced.<sup>[2]</sup> Nevertheless,

the unique characteristics of NPs may not be necessarily benign. Indeed, the potential environmental/health risks of NPs have attracted increasing concern. Extensive nanosafety studies have thus been performed at different biological levels.<sup>[3,4]</sup> For both nanobiotechnology applications and nanosafety evaluations, the ability to directly identify and visualize NPs in target organisms has long been pursued but remains challenging. Currently, the technique most frequently used for these purposes is electron microscopy with ultraspatial resolution down to the sub-nano scale.<sup>[5]</sup> However, the sample preparation, sectioning, and staining processes are laborious and have a high risk of artifacts. Confocal fluorescence microscopy is another common method to examine the subcellular distribution of NPs.<sup>[6]</sup> But it requires that the particles are photoluminescent and fluorescence quenching is a persistent problem.

Other imaging techniques, such as synchrotron-radiation-based spectroscopy, radioautography, and magnetic resonance imaging, are also available with limited applications.<sup>[7,8]</sup>

Raman scattering (RS) microscopy is a nonstaining-dependent, nondestructive, and noninvasive technique that allows direct observation of biomolecules in cells and tissues.<sup>[9]</sup> However, the Raman imaging process is time-consuming and suffers from the strong autofluorescence background of most samples. Coherent anti-Stokes RS (CARS)<sup>[10]</sup> and stimulated RS (SRS)<sup>[11–13]</sup> overcome these problems by stimulating the Raman transition of biomolecules via nonlinear interactions with two coherent pulse laser beams.<sup>[14–16]</sup> As label-free imaging methods, both CARS and SRS have been successfully used in a broad spectrum of applications, including the molecular imaging of cell metabolites,<sup>[17,18]</sup> real-time monitoring of drug delivery,<sup>[19]</sup> differentiating tumor margins from healthy tissues,<sup>[20]</sup> and visualizing specially designed polymer dots in cells via various Raman tags.<sup>[21]</sup> With the latest technical advances in hyperspectral SRS, the chemical mapping of molecules and thus the metabolic fingerprinting of multiple molecular species have become possible.<sup>[19,22–24]</sup> Nevertheless, direct visualization and quantification of dissimilar NPs in single cells by hyperspectral SRS have not been evaluated.

The present study is the first to use hyperspectral SRS to investigate the accumulation and subcellular distribution of dissimilar NPs in unicellular (single-celled) organisms. For this purpose, polyacrylate (PAA)-coated hematite (HemNPs,

Dr. B. Huang, Prof. L. Xiao, Prof. R. Ji, Prof. L. Yang, Prof. A.-J. Miao  
State Key Laboratory of Pollution Control and Resource Reuse  
School of the Environment  
Nanjing University  
Nanjing 210023, Jiangsu Province, China  
E-mail: miaoaj@nju.edu.cn

S. Yan, Prof. P. Wang  
Britton Chance Center for Biomedical Photonics  
Wuhan National Laboratory for Optoelectronics  
Huazhong University of Science and Technology  
Wuhan, Hubei 430074, China  
E-mail: p\_wang@hust.edu.cn

S. Yan, Prof. P. Wang  
MoE Key Laboratory for Biomedical Photonics  
Collaborative Innovation Center for Biomedical Engineering  
School of Engineering Sciences  
Huazhong University of Science and Technology  
Wuhan, Hubei 430074, China

 The ORCID identification number(s) for the author(s) of this article can be found under <https://doi.org/10.1002/sml.201703246>.

DOI: 10.1002/sml.201703246

formula:  $\alpha\text{-Fe}_2\text{O}_3$ ) and anatase (AnaNPs, formula:  $\text{TiO}_2$ ) NPs were selected as representative NPs because of their wide applications in various fields.<sup>[25,26]</sup> As a free-living eukaryotic ciliate, *Tetrahymena thermophila* was used as the target organism considering its ability to internalize particles. Although most nanobiotechnological and nanotoxicological studies have focused on the behavior and effects of only a single type of NPs, this is rarely the case in real applications or in the natural world, where a mixture of NPs is commonly detected. Therefore, potential interactions between HemNPs and AnaNPs during their uptake by *T. thermophila* were also examined.

## 2. Results and Discussion

### 2.1. Physicochemical Characterization of AnaNPs and HemNPs

HemNPs and AnaNPs were surface-coated by PAA with a molecular weight of 2000 and  $1.2 \times 10^6$ , respectively.<sup>[25,26]</sup> Since PAA has a  $\text{p}K_a$  of 4.75,<sup>[27]</sup> HemNPs and AnaNPs were negatively charged in the exposure medium ( $\text{pH} = 6.9$ ), with a zeta potential of  $-19.9$  and  $-25.4$  mV, respectively. Their isoelectric point was 2.0 and 2.7, respectively.<sup>[25,26]</sup> Thus, under the study conditions the HemNPs and AnaNPs were well dispersed and their hydrodynamic particle sizes remained unchanged during the experimental period (35.2–37.2 and 40.2–52.0 nm, respectively; Figure S1a, Supporting Information) due to electrostatic and steric (electrosteric) repulsions between particles. For the same reason, no heteroaggregation occurred when HemNPs and AnaNPs were mixed at different ratios. Accordingly, the average hydrodynamic size, as measured by dynamic light scattering (DLS) was 36.2–50.2 nm, i.e., between the values of

either preparation alone (Figure S1a, Supporting Information). Consistent with the DLS results, the particle size of HemNPs and AnaNPs as determined from the transmission electron microscopy (TEM) images was 10.4 and 16.2 nm, respectively, and there were no direct interactions between the two types of NPs (Figure S1b, Supporting Information). Nevertheless, since a variety of factors, such as pH, ionic strength, cations, and organic matter, may play critical roles in NP–NP interactions,<sup>[28]</sup> substantial heteroaggregation between HemNPs and AnaNPs may still occur when the ambient environmental conditions change. For instance, Tong et al.<sup>[29]</sup> found significant heteroaggregation between negatively charged ZnO and  $\text{TiO}_2$  NPs. It was postulated that electrostatic repulsion was overcome by an increased frequency of collision of the two types of NPs when present in mixtures, a result of the combined effects of surface charge screening and divalent cation bridging.<sup>[30]</sup>

### 2.2. Subcellular Distribution of AnaNPs and HemNPs

Hyperspectral SRS acquires Raman spectra at each pixel of field of view within a few minutes. The advantage of hyperspectral SRS lies in its potential to simultaneously image biomolecules and different NPs in cells.<sup>[31]</sup> The schematic illustration of hyperspectral SRS is shown in Figure 1 with detailed information provided in the Experimental Section. To validate the feasibility of our method, we subjected a mixture of glyceryl trioleate (TAG, as a typical cellular fatty acid), HemNPs, and AnaNPs to SRS imaging in the conventional carbon–hydrogen (C–H) stretching region with a Raman shift from 2800 to 2980  $\text{cm}^{-1}$  (Figure S2a–c, Supporting Information). The SRS spectrum of TAG showed a significant Raman peak at 2850  $\text{cm}^{-1}$  (Figure S2b,

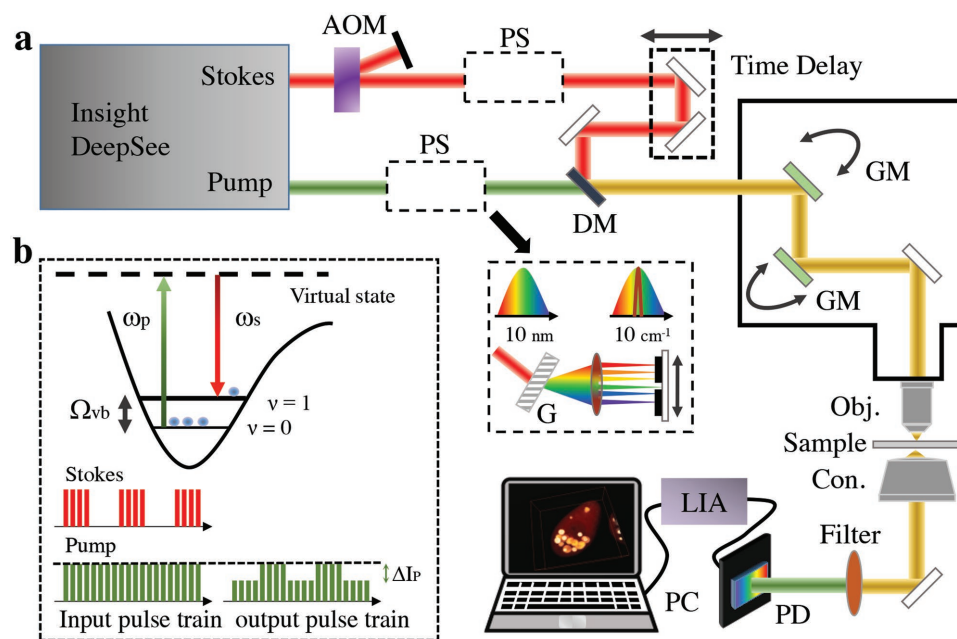


**Figure 1.** Schematic illustration of hyperspectral stimulated Raman scattering (SRS) microscopy. a) Experimental setup. AOM: acousto-optical modulator; PS: pulse shaper; DM: dichroic mirror; GM: galvo mirror; Obj.: objective; Con.: condenser; LIA: lock-in amplifier; PD: photodiode. b) Energy diagram of SRS transition process and high-frequency modulation scheme for sensitive heterodyne detection.  $\omega_p$ : pump beam;  $\omega_s$ : Stokes beam;  $\Omega_{vb}$ : the vibrational energy of the target molecule;  $\Delta I_p$ : the stimulated Raman loss of pump beam.

Supporting Information), attributable to the vibrational stretching of  $-\text{CH}_2$  in acyl chain of lipids.<sup>[32]</sup> Raman spectra of AnaNPs, similar to PAA (Figure S2d, Supporting Information), had two pronounced peaks at 2850 and 2930  $\text{cm}^{-1}$  (Figure S2b, Supporting Information), suggesting that these peaks originated from the PAA coating. These distinctive Raman features of PAA provide an intrinsic contrast for AnaNPs when present in a complex system. Despite the fact that HemNPs also possessed PAA coating on the surface, their Raman spectrum in the hyperspectral SRS image was completely different from that of AnaNPs (Figure S2b, Supporting Information). In this case, the strong and broadband pump-probe signal from  $\alpha\text{-Fe}_2\text{O}_3$  core was overwhelming and dominated over the SRS spectra features from their PAA coating. Such pump-probe signal originates from the electronic transition of  $\alpha\text{-Fe}_2\text{O}_3$ . It depends on the intensity of the laser but is independent of the laser wavelength and the Raman shift. This is in contrast to the SRS signal, which comes from the molecular vibration and requires frequency difference between the pump and probe lasers to match the molecular vibration. The ability of the pump and probe lasers to induce the electronic transition of  $\alpha\text{-Fe}_2\text{O}_3$  but not that of  $\text{TiO}_2$  was further evidenced by the absorption spectra of both NPs (Figure S2e, Supporting Information) as obtained by the UV-vis spectroscopy. A broad absorption band from 400 to 1100 nm was found for HemNPs but not for AnaNPs. Nevertheless, the pump-probe signal of  $\alpha\text{-Fe}_2\text{O}_3$  could be separated from the overlapping SRS spectrum using a multivariate curve resolution (MCR) algorithm,<sup>[24]</sup> as described in the Experimental Section. These data collectively demonstrate the applicability of hyperspectral SRS microscopy and MCR analysis in the chemical mapping of mixed nanomaterials.

Using hyperspectral SRS, the subcellular distribution of the NPs in *T. thermophila* preexposed to HemNPs and AnaNPs at concentrations of 30 mg Fe  $\text{L}^{-1}$  and 13.2 mg Ti  $\text{L}^{-1}$ , respectively, and a mixture of the two NP types was examined. As seen in Figure 2a,d, the shape of the ciliate cell was visualized by the protein signal (purple),<sup>[24]</sup> which was interspersed with tiny spots representing lipid droplets (red). AnaNPs (green) were concentrated mainly in the food vacuoles of *T. thermophila* (Figure 2a). Although AnaNPs were also detected as tiny spots in the cytoplasm, their amount was very limited, as the SRS spectrum of most cytoplasmic region was almost the same as that of the nucleus and proteins had a dominant contribution in both compartments (Figure S3a,c,e, Supporting Information). Unlike the AnaNPs, HemNPs were characterized by a significant distribution in the cytoplasm besides their accumulation in vacuoles (Figure 2b,d). In this case, the SRS spectrum of the cytoplasm was intermediate to that of proteins in the nucleus and HemNPs in food vacuoles (Figure S3b,d,f, Supporting Information).

When the cells were exposed to a mixture of 30 mg Fe  $\text{L}^{-1}$  HemNPs and 13.2 mg Ti  $\text{L}^{-1}$  AnaNPs, their hyperspectral SRS imaging hardly shows any AnaNPs in food vacuoles (Figure 2c–e), as in contrast to the observations from the TEM images (Figure 3a). Such discrepancy was mainly due to the overwhelmed Raman spectrum of AnaNPs by the pump-probe signal of HemNPs when both NPs were present simultaneously in the same subcellular compartments. Nevertheless, AnaNPs could still be seen as tiny spots outside the food vacuoles (green spots

in Figure 2c), where the accumulation of HemNPs was completely suppressed. Further, the signal intensity of the HemNPs in food vacuoles decreased and no HemNPs was observed in the cytoplasm in the presence of AnaNPs, in contrast to their localization in cells exposed to HemNPs alone (Figure 2b). These findings indicate that AnaNPs may inhibit the bioaccumulation of HemNPs, as further discussed below. The accumulation of both NPs in the food vacuoles of *T. thermophila* was also evidenced by the TEM images of cells preexposed to either HemNPs at a concentration of 30 mg Fe  $\text{L}^{-1}$  or AnaNPs at a concentration of 13.2 mg Ti  $\text{L}^{-1}$  (Figure 3b,c). The elemental composition of the areas of interest, as determined by energy dispersive spectroscopy, is shown in Figure S4 (Supporting Information). When *T. thermophila* was exposed to HemNPs alone, the NPs were found in both the food vacuoles and the cytoplasm (Figure 3b), supporting the hyperspectral SRS findings of HemNPs (Figure 2b). Although hyperspectral SRS also showed AnaNPs in small amounts outside the food vacuoles, this was not confirmed by the TEM images, suggesting that SRS is more sensitive than TEM. Taken together, the distinct subcellular distribution of HemNPs and AnaNPs, as visualized by hyperspectral SRS, implies the uptake of the two types of NPs by different routes in *T. thermophila*.

### 2.3. Uptake Routes of AnaNPs and HemNPs

Although many details are lacking, it is generally accepted that only defined areas on the surface of ciliate cells serve as sites for endocytic uptake, since most of the internal aspect of the cell surface is covered by an extensive system of cortical alveoli and the underlying membrane skeleton.<sup>[33]</sup> *T. thermophila* maintains at least four distinct pathways of endocytic uptake, with the two most well-known being phagocytosis through the oral apparatus (OA), a complex funnel-like structure located a short distance posterior to the anterior cell pole, and clathrin-mediated endocytosis (CME) at parasomal sacs just anterior to each ciliary basal body of *T. thermophila*. To further study the internalization routes of HemNPs and AnaNPs, we determined the uptake kinetics of both in the presence of cytochalasin B, colchicine, methyl- $\beta$ -cyclodextrin (M $\beta$ CD), and genistein. Cytochalasin B suppresses the polymerization of actin and the interaction of actin filaments.<sup>[34]</sup> It thus inhibits actin-dependent phagocytosis and macropinocytosis but has no effect on actin-independent endocytic pathways. By binding with tubulin, one of the main constituents of microtubules, colchicine interferes with microtubule transport and thus serves as a microtubule-dependent inhibitor of pinocytosis.<sup>[35]</sup> M $\beta$ CD is a cyclic heptasaccharide that depletes cholesterol and modifies cholesterol-rich domains within the cell membrane;<sup>[36]</sup> it is therefore often used as a selective inhibitor of caveolae-mediated uptake,<sup>[37]</sup> although its suppression of macropinocytosis and CME has also been reported.<sup>[38,39]</sup> As a depressor of several tyrosine kinases, genistein mainly prevents CME and caveolae-mediated endocytosis.<sup>[40]</sup>

The preexposure of *T. thermophila* to the above-described inhibitors resulted in differences in the subsequent uptake of HemNPs and AnaNPs by the ciliate. The uptake rate of AnaNPs was significantly ( $p < 0.05$ ) reduced in the presence

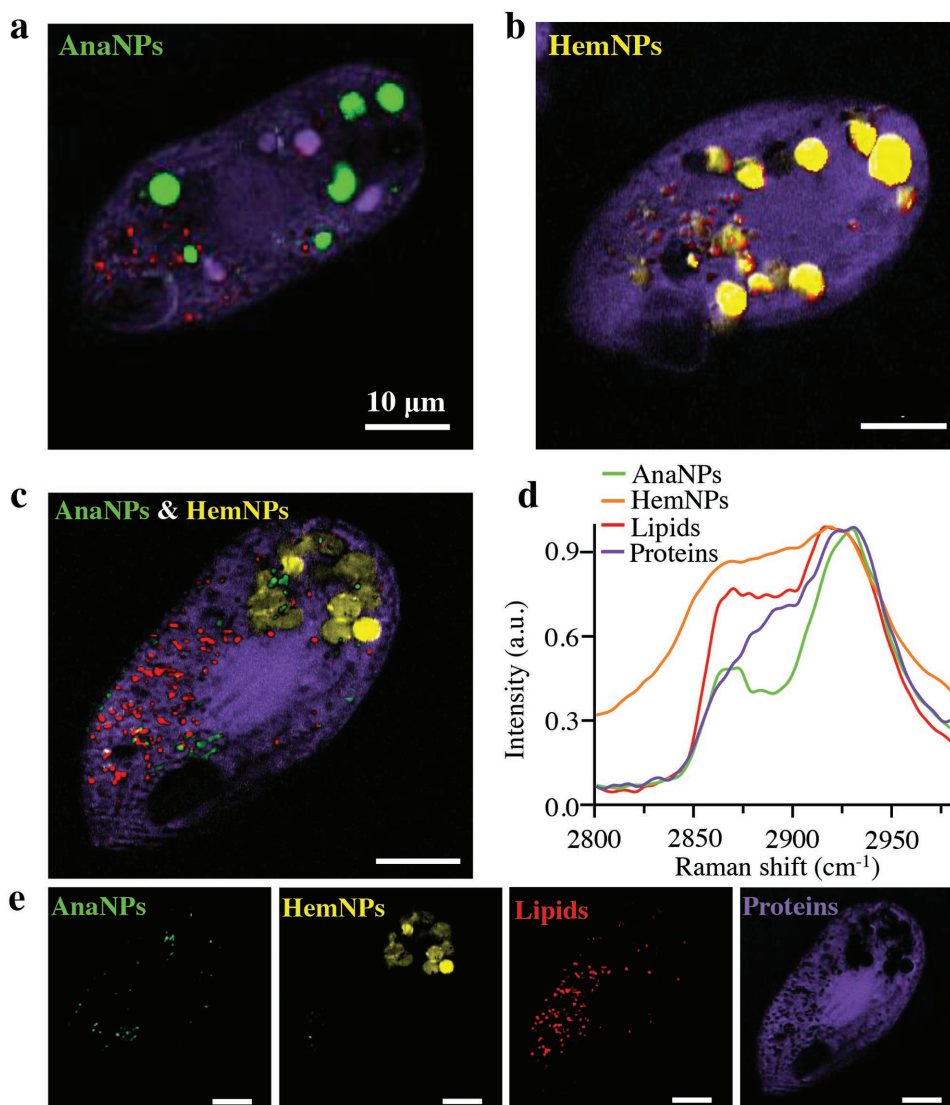


**Figure 2.** Compositional analysis of the subcellular compartments of *T. thermophila* by hyperspectral SRS and multivariate curve resolution (MCR) analysis. MCR-retrieved concentration maps of AnaNPs (green), HemNPs (yellow), lipids (red), and proteins (purple) in *T. thermophila* preexposed to a) AnaNPs ( $13.2 \text{ mg Ti L}^{-1}$ ), b) HemNPs ( $30 \text{ mg Fe L}^{-1}$ ), or c) a mixture of both. d) MCR-retrieved Raman spectra of AnaNPs, HemNPs, lipids, and proteins in (c). e) MCR-reconstructed concentration images of AnaNPs, HemNPs, lipids, and proteins in (c).

of cytochalasin B, but was unaffected by colchicine, M $\beta$ CD, and genistein (Table 1). By contrast, the uptake rate of HemNPs was significantly ( $p < 0.05$ ) decreased after the preexposure of the ciliate to all four inhibitors (Table 1). Considering the size of the vesicles involved in the internalization of AnaNPs and HemNPs (Figures 2 and 3), the inhibitor results imply that the uptake of AnaNPs by *T. thermophila* is predominantly through phagocytosis, while both phagocytosis and pinocytosis (most likely CME) are involved in HemNP internalization (Figure S5, Supporting Information). The phagocytosis of HemNPs and AnaNPs as observed herein was consistent with the above-described hyperspectral SRS and TEM results, both of which showed the accumulation of NPs in the food vacuoles of *T. thermophila*. The involvement of pinocytosis in the uptake of HemNPs but not AnaNPs is also consistent with the aforementioned different cellular distribution patterns of these two particle types outside the

food vacuoles. Thus, PAAs with different molecular weights may have completely different binding affinities with the pinocytosis-related receptors on the cell membrane. Alternatively, potential effects from the different cores of HemNPs and AnaNPs on their different uptake routes cannot be excluded.

#### 2.4. Uptake Competition between AnaNPs and HemNPs

Since phagocytosis was involved in the internalization of both AnaNPs and HemNPs, potential interactions between these two NPs during their uptake by *T. thermophila* were expected and thus examined by SRS in the present study. For this purpose, *T. thermophila* was exposed for 2 h to a fixed concentration of HemNPs ( $30 \text{ mg Fe L}^{-1}$ ) together with AnaNPs at concentrations of 0, 0.4, 1.3, 4, or  $13.2 \text{ mg Ti L}^{-1}$ , respectively. A control treatment

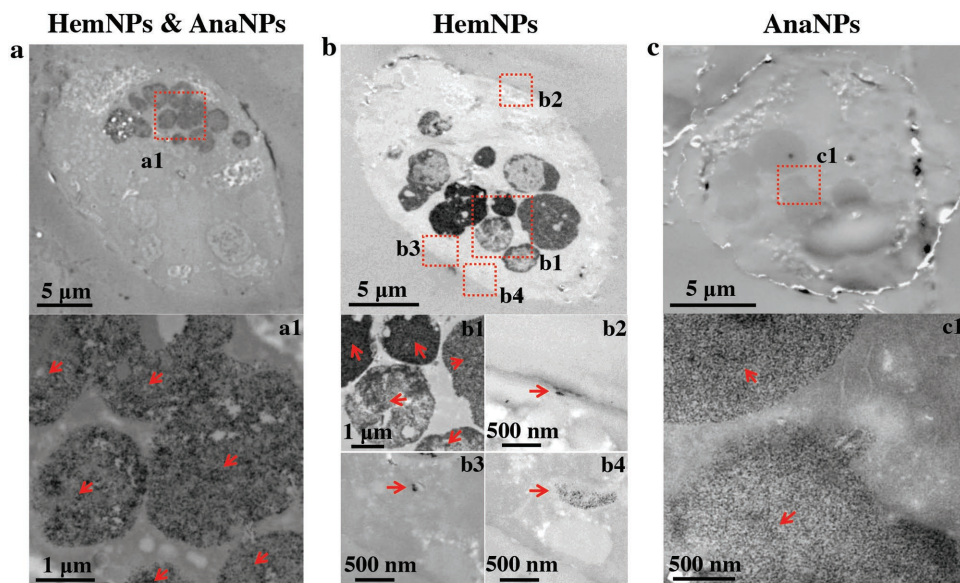


**Figure 3.** TEM images of *T. thermophila* cell slices. The cells were preexposed to a) a mixture of HemNPs ( $30 \text{ mg Fe L}^{-1}$ ) and AnaNPs ( $13.2 \text{ mg Ti L}^{-1}$ ), b) HemNPs ( $30 \text{ mg Fe L}^{-1}$ ) only, or c) AnaNPs ( $13.2 \text{ mg Ti L}^{-1}$ ) only. a1, b1–b4, c1) Magnified images of the areas outlined by the dotted rectangle in (a–c). Arrows indicate the accumulation of HemNPs, AnaNPs, or both as verified by energy dispersive X-ray spectrometry (Figure S4, Supporting Information).

without any addition of HemNPs and AnaNPs was also included. The large-field-of-view of the pump-probe images of cells at varying AnaNP concentrations is shown in Figure 4a, together with the corresponding zoom-in images of representative cells (Figure 4b,c). When the wavelength of pump laser was kept at 802 nm, the overall C-H vibration from the protein and lipid molecules revealed the shape of the cell (Figure 4b). To quantify the concentration of HemNPs in *T. thermophila*, the wavelength was increased from 802 to 840 nm and the relative Raman shift from the Stokes laser was  $\approx 2300 \text{ cm}^{-1}$ . Under this condition, SRS imaging enters the vibrational silence region such that only the pump-probe signal was detected. Therefore, the signals from the ciliate's proteins and lipids disappeared

and no signal was found in cells not exposed to HemNPs (control treatment, Figure 4a,c). By contrast, a significant HemNP signal was obtained when the cells were exposed to HemNPs alone at a concentration of  $30 \text{ mg Fe L}^{-1}$  (Figure 4a,c). In this case, the NPs were distributed throughout the cytoplasm but not in the nucleus, with the highest concentration in food vacuoles. A substantial amount of HemNPs was also attached to the cilia on the cell membrane. The subcellular distribution pattern of HemNPs was further indicated in the reconstructed 3D image of *T. thermophila* (Figure S6 and Movie S1, Supporting Information) as obtained by SRS.

More interestingly, the HemNP signal of all cells within the large-field-of-view gradually decreased with increasing

**Table 1.** Suppression of HemNP and AnaNP uptake by *Tetrahymena thermophila* preexposed to  $0.1 \times 10^{-3} \text{ M}$  cytochalasin B (cyt B),  $12.5 \times 10^{-3} \text{ M}$  colchicine,  $30 \times 10^{-3} \text{ M}$  M $\beta$ CD, or  $10 \times 10^{-6} \text{ M}$  genistein, respectively.

NPs	Inhibitor	Inhibition [%]	Phagocytosis (>1 $\mu\text{m}$ ) <sup>a)</sup>	Pinocytosis			
				Macropinocytosis (>0.5 $\mu\text{m}$ )	Clathrin mediated ( $\approx 120 \text{ nm}$ )	Caveolae mediated ( $\approx 50\text{--}80 \text{ nm}$ )	Clathrin/caveolae independent ( $\approx 90 \text{ nm}$ )
HemNPs	Colchicine	62.5% <sup>b)</sup>		+ <sup>c)</sup>	+	+	
	cyt B	30.5% <sup>b)</sup>	+	+			
	M $\beta$ CD	55.9% <sup>b)</sup>		+	+	+	
	Genistein	33.7% <sup>b)</sup>			+	+	
AnaNPs	Colchicine	–1.4%		– <sup>d)</sup>	–	–	
	cyt B	54.3% <sup>b)</sup>	+	+			
	M $\beta$ CD	–0.5%		–	–	–	
	Genistein	–2.6%			–	–	

<sup>a)</sup>The size of the vesicles involved in this endocytosis route; <sup>b)</sup> $p < 0.05$ ; <sup>c)</sup>This endocytosis route could be suppressed by the inhibitor in the same row and significant uptake inhibition was observed; <sup>d)</sup>This endocytosis route could be suppressed by the inhibitor in the same row but no significant uptake inhibition was observed.

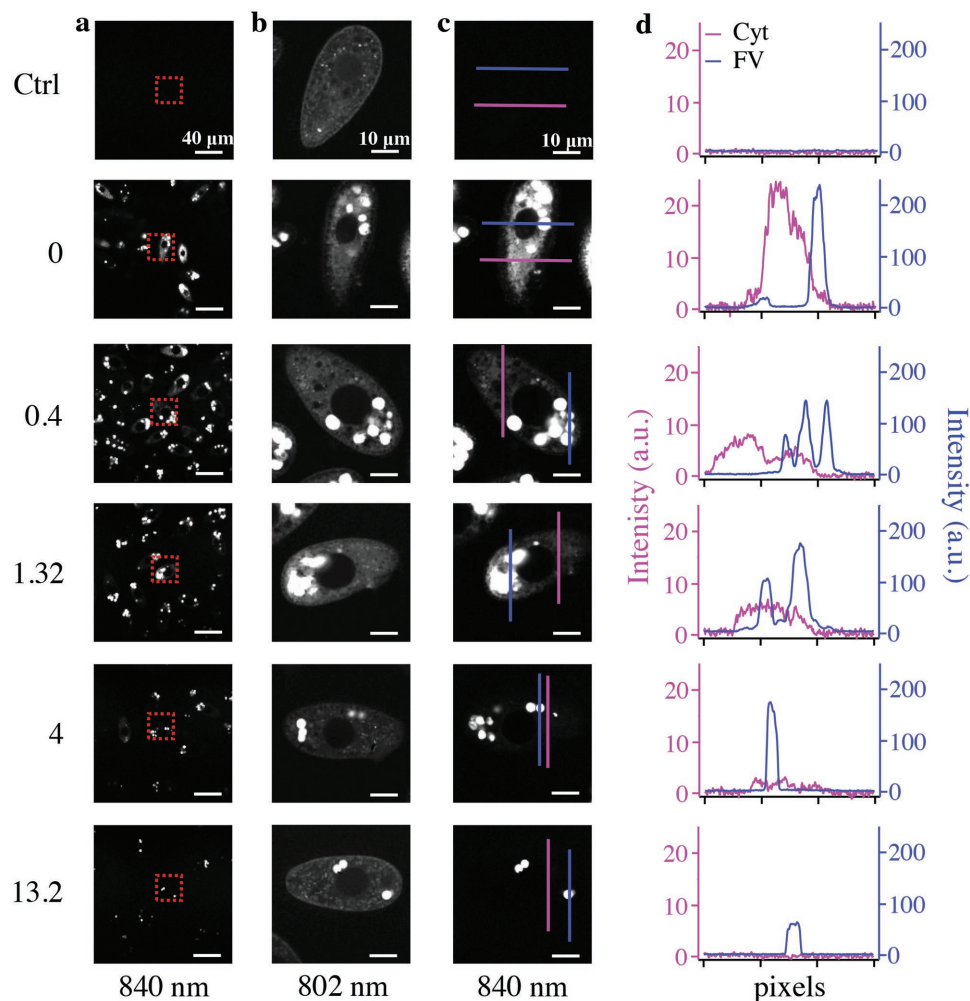


**Figure 4.** SRS imaging of *T. thermophila*. a) The large-field-of-view image of *T. thermophila* acquired with a pump laser wavelength of 840 nm. b,c) The magnified images of the areas outlined by the dotted rectangle in (a). The pump laser wavelength used to acquire images in (b) and (c) was 802 and 840 nm, respectively. d) The intensities of the pump-probe signal of HemNPs along the pink and blue lines, which cross the cytoplasm (Cyt) and food vacuoles (FV), respectively. The cells were cultured in medium without any addition of both NPs (Ctrl) or with the addition of HemNPs ( $30 \text{ mg Fe L}^{-1}$ ) in the presence of AnaNPs at concentrations of 0, 0.4, 1.32, 4, and  $13.2 \text{ mg Ti L}^{-1}$ , respectively, for 2 h.

concentrations of AnaNPs in the exposure medium (Figure 4a). At the highest AnaNP concentration, the HemNPs signal was only visible in food vacuoles at a much lower intensity. Accordingly, peak values of HemNPs in both the cytoplasm and food vacuoles decreased as the concentration of AnaNPs increased, based on the concentration profiles of HemNPs across the cytoplasm (pink line) and food vacuoles (blue line) (Figure 4d). We then quantified the pump-probe signal of HemNPs for the large-field-of-view cells in different AnaNP concentration treatments (Figure 4a), using ImageJ. Its relative change compared to the treatment without AnaNP addition decreased hyperbolically with increasing concentrations of AnaNPs (Figure 5a), as was well simulated by a two-site competition model (Equation (S1), “Two-site Competition Model,” Supporting Information).<sup>[41]</sup> This finding suggests that AnaNPs suppressed the uptake of HemNPs through at least two distinct mechanisms: (1) not only by competitively inhibiting the phagocytosis of HemNPs, (2) but also by noncompetitively decreasing the

cell-surface adsorption of these particles and their subsequent internalization through pinocytosis.

To further verify the remarkable accumulation of both NP types in *T. thermophila* as well as the inhibitive effects of AnaNPs on the accumulation of HemNPs, the uptake kinetics of HemNPs at different concentrations of AnaNPs ( $[\text{AnaNPs}]_{\text{med}}$ ) was examined in a conventional biokinetics analysis (Experimental Section). Although the Raman signal of AnaNPs was overwhelmed by the pump-probe signal of HemNPs, which prevented a determination of the effects of HemNPs on the accumulation of AnaNPs via SRS, this was not an issue in the biokinetics study. Therefore, the uptake kinetics of AnaNPs at different concentrations of HemNPs ( $[\text{HemNPs}]_{\text{med}}$ ) was also studied. During the 2 h uptake period, both the cellularly accumulated concentrations of HemNPs ( $[\text{HemNPs}]_{\text{cell}}$ ) and AnaNPs ( $[\text{AnaNPs}]_{\text{cell}}$ ) increased linearly with exposure time, regardless of whether uptake was examined in the presence or absence of dissimilar NPs (Figure S7, Supporting Information).

The increase was not due to the consecutive adsorption of NPs on the cell surface, which was completed within 15 min of exposure according to our finding that  $[\text{HemNPs}]_{\text{cell}}$  of heat-killed or cold-treated cells remained constant throughout the exposure period (Figure S8, Supporting Information). The endocytosis by these heat-killed or cold-treated cells ceased and their NP accumulation should have proceeded by surface adsorption only. Similar to HemNPs, the accumulation of AnaNPs by heat-killed or cold-treated *T. thermophila* also remained unchanged with exposure time, as previously reported in a study from our group.<sup>[25]</sup>

A comparison of the uptake kinetics of HemNPs and AnaNPs revealed a significant intercept, as an indicator of NP surface adsorption, for HemNPs while the intercept obtained from the uptake kinetics of AnaNPs was close to zero. This adsorption difference between HemNPs and AnaNPs was consistent with their subcellular distributions and uptake mechanisms as determined in the above-described SRS and inhibitor experiments (Figure S5, Supporting Information). Since AnaNPs were taken up mainly through phagocytosis and their cell-surface attachment is a prerequisite for uptake,<sup>[42]</sup> the negligible cell-surface adsorption of AnaNPs indicates that the OA of *T. thermophila* was the only site to which these particles attached before their internalization. Since the OA accounts for only a small fraction of the total area of the cell surface, the number of NPs attached to it would presumably have been below the detection limit in the uptake kinetics experiment. In contrast to AnaNPs, the cell-surface adsorption of HemNPs was substantial, as these particles attach not only to the OA but also to pinocytosis receptors distributed all over the cell surface.

Besides the difference in cell-surface adsorption between HemNPs and AnaNPs, their mutual presence in the uptake media decreased their respective accumulation (Figure S7, Supporting Information). Thus,  $[\text{HemNPs}]_{\text{cell}} ([\text{AnaNPs}]_{\text{cell}})$  declined with the increase in  $[\text{AnaNPs}]_{\text{med}} ([\text{HemNPs}]_{\text{med}})$  at each time point during the 2 h uptake period. The inhibitory effects of dissimilar NPs on the bioaccumulation (both cell-surface adsorption and internalization) of either HemNPs or AnaNPs were more obvious when the uptake rates and cell surface adsorption of the particles were calculated (Figure 5b and Figure S9, Supporting Information). The hyperbolic correlation between uptake rate or cell-surface adsorption of HemNPs and  $[\text{AnaNPs}]_{\text{med}}$  as well as that between the AnaNP uptake rate and  $[\text{HemNPs}]_{\text{med}}$  (Figure 5b and Figure S9, Supporting Information) could also be simulated by the two-site competition model (Equations (S2)–(S4), “Two-site Competition Model,” Supporting Information), further supporting our hypothesis of the involvement of at least two distinct mechanisms in the uptake competition between HemNPs and AnaNPs. Although AnaNPs did not attach to pinocytosis receptors, they may still have been able to inhibit HemNP collision and binding to these sites.<sup>[43]</sup> Further considering the close links between the various forms of endocytosis and that a decrease in one form may be accompanied by a proportional increase in another,<sup>[33]</sup> the inhibition of NP uptake in the presence of dissimilar NPs may be a combined effect of these linkages and the competition for cell-surface attachment.

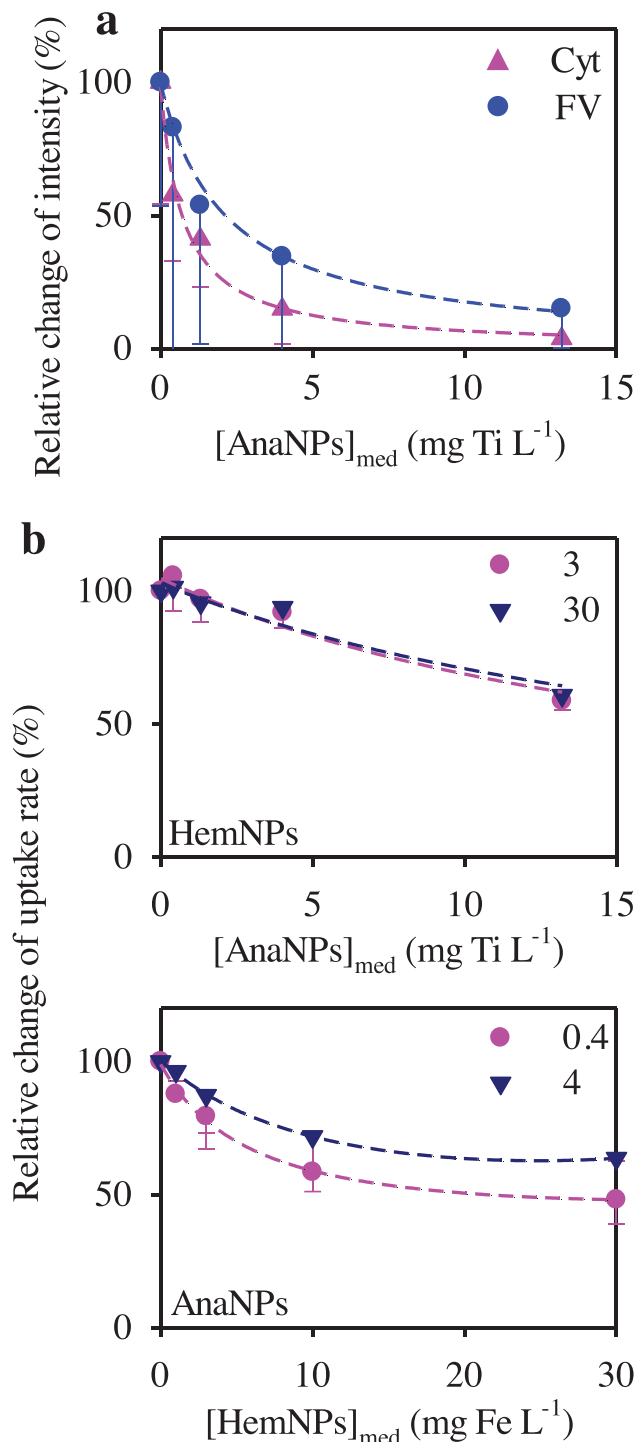


**Figure 5.** Uptake competition between HemNPs and AnaNPs. a) Relative change in the intensities of the pump-probe signal from HemNPs in the cytoplasm (Cyt) and food vacuoles (FV) of *T. thermophila* at different ambient concentrations of AnaNPs ( $[\text{AnaNPs}]_{\text{med}}$ ). The cells were preexposed to HemNPs ( $30 \text{ mg Fe L}^{-1}$ ) in the presence of increasing concentrations of AnaNPs ( $0, 0.4, 1.32, 4, \text{ and } 13.2 \text{ mg Ti L}^{-1}$ ). b) Top: relative change in the uptake rate of HemNPs ( $3 \text{ and } 30 \text{ mg Fe L}^{-1}$ ) with increasing concentrations of AnaNPs ( $0, 0.4, 1.32, 4, \text{ and } 13.2 \text{ mg Ti L}^{-1}$ ); bottom: relative change in the uptake rate of AnaNPs ( $0.4 \text{ and } 4 \text{ mg Ti L}^{-1}$ ) with increasing concentrations of HemNPs ( $0, 1, 3, 10, \text{ and } 30 \text{ mg Fe L}^{-1}$ ). Data are presented as the mean  $\pm$  standard deviations ( $n = 3$ ).

### 3. Conclusions

In summary, our study demonstrates the use of hyperspectral SRS as a powerful tool for both qualitative and quantitative analyses of the uptake routes and target sites of different NPs in single cells. The ability of this label-free imaging technique to provide chemical images of cells at submicron resolution is clearly shown. Thus, hyperspectral SRS can be used to improve our understanding of the adsorption, metabolism, distribution, accumulation, and elimination of NPs inside cells and therefore to shed light on the intracellular interactions between NPs and biomolecules. Further, in combination with a conventional biokinetics experiment, hyperspectral SRS imaging revealed the uptake competition between dissimilar NPs, which should be considered not only in medical/biological applications but also in safety assessments of NPs.

### 4. Experimental Section

**NPs and Organism:** HemNPs (primary particle size 5–10 nm) were synthesized by titration hydrolysis and a precipitation–redispersion process was used in their PAA coating. Detailed information on the synthesis of HemNPs can be found in Huang et al.<sup>[26]</sup> In determination of [HemNPs]<sub>cell</sub>, <sup>55</sup>Fe-labeled HemNPs (specific activity  $8 \times 10^{-4}$  mCi mg<sup>-1</sup>) were used to exclude potential interference from the background and to improve the detection limit of iron.<sup>[26]</sup> AnaNPs (primary particle size 1–10 nm) were purchased from Vive Nano (Toronto, Canada). The crystal structures of the two NP types were verified previously by X-ray diffraction spectroscopy.<sup>[25,26]</sup> The PAA coating accounted for 58% and 74% of the total weight of HemNPs and AnaNPs, respectively. The hydrodynamic sizes of the NPs in the experimental medium, either alone or in a mixture, were determined by a DLS particle sizer (ZetaPALS, Brookhaven Instruments, NY, USA).<sup>[26]</sup> TEM images of the particles in the experimental suspensions were also recorded (JEM-200CX, JEOL, Tokyo, Japan).<sup>[44]</sup>

The ciliate *Tetrahymena thermophila* SB210 (pear-shaped,  $50 \times 20 \mu\text{m}$ ) was a gift from the Institute of Hydrobiology, Chinese Academy of Sciences. A stock culture was maintained axenically at 25 °C in a nutrient-enriched medium containing proteose peptone (2% w/w), yeast extract (0.1% w/w), Fe-EDTA (0.003% w/w), penicillin G (100 units mL<sup>-1</sup>), streptomycin sulfate (100 mg L<sup>-1</sup>), and amphotericin B (0.025 mg L<sup>-1</sup>); the pH was 7.0.<sup>[25]</sup> To rule out potential effects of proteose peptone and yeast extract on the behavior of HemNPs and AnaNPs, a simplified medium (pH = 6.9, ionic strength =  $\approx 20 \times 10^{-3}$  M) consisting of NaH<sub>2</sub>PO<sub>4</sub> ( $2 \times 10^{-3}$  M), Na<sub>2</sub>HPO<sub>4</sub> ( $1 \times 10^{-3}$  M), and CaCl<sub>2</sub> ( $1.5 \times 10^{-3}$  M) was used in all exposure experiments.<sup>[45]</sup> *T. thermophila* was harvested from the culture by centrifugation (1700 RCF, 10 min), with the speed and duration optimized so that the cells could be collected effectively and sedimentation of the NPs was avoided.

**SRS Molecular Imaging:** The *T. thermophila* cells in the experimental medium of the different treatments were directly fixed by paraformaldehyde (final concentration 1% w/v). Subsequently, 1  $\mu\text{L}$  of the fixed sample was added onto a piece of VWR Micro Cover Glass, covered by another one, and directly analyzed by SRS. The hyperspectral SRS microscope (Figure 1) employed a dual-output femtosecond (fs) pulse laser (InSight DeepSee, Spectra-Physics, Mountain View, CA, USA).<sup>[32]</sup> The 120 fs tunable laser with a maximum output power of 1 W served as the pump beam ( $\omega_p$ ); the laser's wavelength was adjustable in the range of 680–1300 nm. The 220 fs laser with a maximum output power of 1.5 W and a fixed wavelength of 1040 nm served as the Stokes beam ( $\omega_s$ ). The repetition rate of both lasers was 80 MHz. For heterodyne detection, the Stokes beam intensity was modulated by an acoustooptical modulator (AOM; 1205-C, Isomet, Springfield, VA) at 2.21 MHz. One 4f pulse shaper (PS) was employed in the Stokes beam to narrow down the

pulse width of the 220 fs laser to 2.3 ps (full width at half-maximum). Another 4f PS was installed in the pump beam for intrapulse wavelength scanning with a motorized translation stage (T-LS28E, Zaber, Vancouver, Canada) at the Fourier plane of the PS. By controlling the slit width, a spectral resolution of  $\approx 0.2$  nm was obtained for the pump beam. The pump and Stokes beams were collinearly combined and directed into a homebuilt laser scanning upright microscope. A water immersion objective lens (UPlanSApo, Olympus, Tokyo, Japan) with a numerical aperture (NA) of 1.2 focused the lasers into the sample. The pump beam was collected by an oil condenser (NA = 1.4) and selected by two bandpass filters (HQ825/150m, Chroma, Bellows Falls, VT). The photons were detected by a photodiode (S3994-01, Hamamatsu, Japan) equipped with a resonant circuit that selectively amplifies the signal at the optical modulation frequency. The stimulated Raman loss signal was then extracted by a digital lock-in amplifier (HF2LI, Zurich Instrument, Zurich, Switzerland), the SRS signal of which was sampled by a DAQ card (PCI 6251, National Instruments, Austin, TX). A Labview platform synchronized wavelength scanning with the stacking of the XY- $\Omega$  ( $\Omega$ : Raman shift) images. Hyperspectral SRS imaging was performed by varying the Raman shift from 2800 to 2980 cm<sup>-1</sup>, which covered the C-H stretching bands of proteins, lipids, and the PAA coatings of HemNPs and AnaNPs. Each SRS image comprised at least  $200 \times 200$  pixels. To quantify the concentration of HemNPs based on the pump-probe signal from  $\alpha\text{-Fe}_2\text{O}_3$ , the wavelength of the pump laser was tuned to 840 nm, where the Raman spectrum is within the silence region. The ability to quantify HemNPs by their pump-probe signal was proved through a control experiment as shown in Figure S10a,b (Supporting Information), where a linear correlation between HemNP concentration and their pump-probe signal was observed. Further, the pump-probe signal of HemNPs was quite stable without any photo bleaching after 100 imaging frames ( $\approx 100$  s) (Figure S10c, Supporting Information), which is not the case for conventional spontaneous Raman spectroscopy (Figure S10d, Supporting Information).

After SRS data acquisition, the MCR algorithm was used to decompose the XY- $\Omega$  spectral data set **D** into concentration profiles and the spectra of the chemical components (Figure S11, Supporting Information),<sup>[46,47]</sup> represented by matrices **C** and **S**<sup>T</sup>

$$\mathbf{D} = \mathbf{C} \cdot \mathbf{S}^T + \mathbf{E} \quad (1)$$

where **T** is the transpose of the matrix **S**; **E** is the residual matrix or experimental error; the input to MCR is the data set **D** and the reference spectrum of each component; and **S** contains the output spectra of all fitted components. The output concentration of a chemical component at each pixel is expressed as the percentage relative to the intensity of the MCR-optimized spectrum. Based on an initial estimate of the pure spectra either from principal component analysis or prior knowledge, an alternating least squares algorithm calculates **C** and **S** by Equation (1) iteratively until the results optimally fit the data matrix **D**.

**TEM Analyses of the Cell Sample:** Similar to the procedure described in a previous study,<sup>[48]</sup> *T. thermophila* was fixed with 1.25% glutaraldehyde in phosphate-buffered saline (0.2 M) after a 2 h exposure to HemNPs (30 mg Fe L<sup>-1</sup>), AnaNPs (13.2 mg Ti L<sup>-1</sup>), or mixtures thereof. The cells were then stained in 1% osmium tetroxide, dehydrated with graded acetone solutions (30, 50, 70, 80, 90, and  $2 \times 100\%$ ) for 10 min each, embedded in epoxy resin, and sectioned. Leaving the cells unstained with heavy metal stains (e.g., uranyl acetate and lead citrate) facilitated NP detection inside the cells. The elemental composition of potential HemNP- and AnaNP-containing spots in the TEM samples was determined by energy-dispersive X-ray spectrometry (JEM-2100, JEOL, Tokyo, Japan).

**Inhibitor Experiments:** The mechanisms underlying the uptake of HemNPs and AnaNPs were elucidated using four pharmacological inhibitors (cytochalasin B, colchicine, M $\beta$ CD, and genistein). *T. thermophila* cells were first exposed to cytochalasin B ( $0.1 \times 10^{-3}$  M), colchicine ( $12.5 \times 10^{-3}$  M), M $\beta$ CD ( $30 \times 10^{-3}$  M), or genistein ( $10 \times 10^{-6}$  M) for 1 h, after which their uptake of HemNPs (30 mg Fe L<sup>-1</sup>) and AnaNPs (4 mg Ti L<sup>-1</sup>) was investigated. The uptake of HemNPs and AnaNPs by inhibitor-unexposed cells served as the control treatment. The cell density of *T. thermophila* in the uptake media was maintained at  $0.8\text{--}1 \times 10^5$  cells mL<sup>-1</sup>.

The uptake experiment lasted for 2 h, during which subsamples were taken at 0.5, 1, 1.5, and 2 h. At each time point, *T. thermophila* cells from 10 mL of culture medium were collected by centrifugation and digested in nitric acid.<sup>[26]</sup> Subsequently, the radioactivity of <sup>55</sup>Fe-labeled HemNPs was determined by liquid scintillation counting (LSC, Tri-Carb 2800 TR, PerkinElmer, USA), using Permafluor cocktail (PerkinElmer) as the scintillator. The cellular accumulation of HemNPs was calculated using Equation (2)

$$[\text{HemNPs}]_{\text{cell}} = \frac{\text{Radioactivity per cell} \times [\text{HemNPs}]_{\text{med}}}{\text{Radioactivity per liter experimental medium}} \quad (2)$$

As for AnaNPs, the cells collected at each time point were digested in sulfuric acid and ammonium sulfate.<sup>[25]</sup> [AnaNPs]<sub>cell</sub> was then quantified by graphite furnace atomic absorption spectrometry (Thermo Fisher Scientific Inc., Waltham, MA, USA). Thereafter, the uptake rate was calculated as the slope of the linear regression between [HemNPs]<sub>cell</sub> or [AnaNPs]<sub>cell</sub> and exposure time. As NP adsorption onto the cell surface occurs quickly and is completed within a few minutes,<sup>[25,49]</sup> the intercept of the linear regression represents the amount of NPs adsorbed on the cell surface. In addition, [HemNPs]<sub>med</sub> and [AnaNPs]<sub>med</sub> were measured at the beginning and end of the uptake experiment. The initial and final cell densities were also determined using a Z2 Coulter counter (Beckman Coulter Inc., CA, USA).

To ensure that the time-dependent increase in [HemNPs]<sub>cell</sub> was not because of the continuous adsorption of the particles onto the surface of *T. thermophila*, particle uptake by heat-killed and cold-treated cells was quantified. In both situations, the HemNP concentration in the uptake medium was fixed at 1 mg Fe L<sup>-1</sup> and the exposure time at 2 h. Heat-killed cells were obtained by culturing the cells at 55 °C for 3 min before the uptake experiment. As for the cold-treated uptake, HemNP accumulation was monitored at 4 °C. The other procedures were the same as described above for the uptake experiments. Similar experiments were performed for AnaNPs in a previous study and thus were not conducted as part of the present work.

**Uptake Competition between HemNPs and AnaNPs:** Two experiments were conducted to investigate the effects of AnaNPs on HemNP uptake (first experiment) and of HemNPs on AnaNP uptake (second experiment). The first experiment had 10 treatments, including two [HemNPs]<sub>med</sub> (3 and 30 mg Fe L<sup>-1</sup>) and five [AnaNPs]<sub>med</sub> (0, 0.4, 1.3, 4.0, and 13.2 mg Ti L<sup>-1</sup>) in the uptake media. The second experiment also had 10 treatments, two [AnaNPs]<sub>med</sub> (0.4 and 4 mg Ti L<sup>-1</sup>) and five [HemNPs]<sub>med</sub> (0, 1, 3, 10, and 30 mg Fe L<sup>-1</sup>) in triplicate. The other procedure was the same as what was used to examine the uptake kinetics in the inhibitor experiment described above.

**Statistical Analysis:** Significant differences (*p* < 0.05) were based on the results of a one-way or two-way analysis of variance with post-hoc multiple comparisons (Tukey or Tamhane; SPSS 11.0 by SPSS, Chicago, USA). The normality (Kolmogorov–Smirnov and Shapiro–Wilk tests) and homogeneity of variance (Levene's test) of the data were determined during the analysis of variance.

## Supporting Information

Supporting Information is available from the Wiley Online Library or from the author.

## Acknowledgements

B.H. and S.Y. contributed equally to this work. The authors thank Dr. Qiaoguo Tan for his constructive suggestions on this paper. The ciliate is courtesy of Dr. Wei Miao. This work was funded by the National Natural Science Foundation of China (21237001, 21677068, and 41271486), Chinese Public Science and Technology Research funds for ocean projects (201505034) to A.-J.M., and by National Key Research and

Development Program of China (2016YFA0201403), the Recruitment Program of Global Experts, and Director Fund of the Wuhan National Laboratory for Optoelectronics to P.W.

## Conflict of Interest

The authors declare no conflict of interest.

## Keywords

hyperspectral stimulated Raman scattering microscopy, label-free imaging, nanoparticles, uptake competition

Received: September 19, 2017

Revised: November 14, 2017

Published online:

- [1] S. J. Klaine, P. J. Alvarez, G. E. Batley, T. F. Fernandes, R. D. Handy, D. Y. Lyon, S. Mahendra, M. J. McLaughlin, J. R. Lead, *Environ. Toxicol. Chem.* **2008**, *27*, 1825.
- [2] C. M. Niemeyer, C. A. Mirkin, *Nanobiotechnology: Concepts, Applications and Perspectives*, Wiley, Hoboken, NJ, USA **2004**.
- [3] A. López-Serrano, R. M. Olivas, J. S. Landaluz, C. Cámara, *Anal. Methods* **2014**, *6*, 38.
- [4] B. J. Marquis, S. A. Love, K. L. Braun, C. L. Haynes, *Analyst* **2009**, *134*, 425.
- [5] T. M. Mayhew, C. Mühlfeld, D. Vanhecke, M. Ochs, *Ann. Anat.* **2009**, *191*, 153.
- [6] A. Elsaesser, A. Taylor, G. S. de Yanés, G. McKerr, E. M. Kim, E. O'Hare, C. V. Howard, *Nanomedicine* **2010**, *5*, 1447.
- [7] Y. Gao, N. Liu, C. Chen, Y. Luo, Y. Li, Z. Zhang, Y. Zhao, B. Zhao, A. Iida, Z. Chai, *J. Anal. At. Spectrom.* **2008**, *23*, 1121.
- [8] J. Cheon, J. H. Lee, *Acc. Chem. Res.* **2008**, *41*, 1630.
- [9] W. Tipping, M. Lee, A. Serrels, V. Brunton, A. Hulme, *Chem. Soc. Rev.* **2016**, *45*, 2075.
- [10] A. Zumbusch, G. R. Holtom, X. S. Xie, *Phys. Rev. Lett.* **1999**, *82*, 4142.
- [11] E. Ploetz, S. Laimgruber, S. Berner, W. Zinth, P. Gilch, *Appl. Phys. B: Lasers Opt.* **2007**, *87*, 389.
- [12] C. W. Freudiger, W. Min, B. G. Saar, S. Lu, G. R. Holtom, C. He, J. C. Tsai, J. X. Kang, X. S. Xie, *Science* **2008**, *322*, 1857.
- [13] B. G. Saar, C. W. Freudiger, J. Reichman, C. M. Stanley, G. R. Holtom, X. S. Xie, *Science* **2010**, *330*, 1368.
- [14] J. X. Cheng, X. S. Xie, *Science* **2015**, *350*, aaa8870.
- [15] A. Folick, W. Min, M. C. Wang, *Curr. Opin. Genet. Dev.* **2011**, *21*, 585.
- [16] J. X. Cheng, X. S. Xie, *Coherent Raman Microscopy*, Taylor and Francis, NY, USA **2012**.
- [17] W. Min, C. W. Freudiger, S. Lu, X. S. Xie, *Annu. Rev. Phys. Chem.* **2011**, *62*, 507.
- [18] P. Wang, B. Liu, D. Zhang, M. Y. Belew, H. A. Tissenbaum, J. X. Cheng, *Angew. Chem., Int. Ed.* **2014**, *53*, 11787.
- [19] D. Fu, J. Zhou, W. S. Zhu, P. W. Manley, Y. K. Wang, T. Hood, A. Wylie, X. S. Xie, *Nat. Chem.* **2014**, *6*, 614.
- [20] M. Ji, S. Lewis, S. Camelo-Piragua, S. H. Ramkissoon, M. Snuderl, S. Venneti, A. Fisher-Hubbard, M. Garrard, D. Fu, A. C. Wang, *Sci. Transl. Med.* **2015**, *7*, 309ra163.
- [21] F. Hu, S. D. Brucks, T. H. Lambert, L. M. Campos, W. Min, *Chem. Commun.* **2017**, *53*, 6187.
- [22] D. Fu, Y. Yu, A. Folick, E. Currie, R. V. Farese Jr., T. H. Tsai, X. S. Xie, M. C. Wang, *J. Am. Chem. Soc.* **2014**, *136*, 8820.

- [23] Y. Ozeki, W. Umemura, Y. Otsuka, S. Satoh, H. Hashimoto, K. Sumimura, N. Nishizawa, K. Fukui, K. Itoh, *Nat. photonics* **2012**, *6*, 845.
- [24] D. Zhang, P. Wang, M. N. Slipchenko, D. Ben-Amotz, A. M. Weiner, J. X. Cheng, *Anal. Chem.* **2012**, *85*, 98.
- [25] W. W. Yang, Y. Wang, B. Huang, N. X. Wang, Z. B. Wei, J. Luo, A. J. Miao, L. Y. Yang, *Environ. Sci. Technol.* **2014**, *48*, 7568.
- [26] B. Huang, L. Xiao, L. Y. Yang, R. Ji, A. J. Miao, *Environ. Pollut.* **2016**, *213*, 801.
- [27] N. Feng, J. Dong, G. Han, G. Wang, *Macromol. Rapid Commun.* **2014**, *35*, 721.
- [28] A. N. Afrooz, I. A. Khan, S. M. Hussain, N. B. Saleh, *Environ. Sci. Technol.* **2013**, *47*, 1853.
- [29] T. Tong, K. Fang, S. A. Thomas, J. J. Kelly, K. A. Gray, J. F. Gaillard, *Environ. Sci. Technol.* **2014**, *48*, 7924.
- [30] D. P. Stankus, S. E. Lohse, J. E. Hutchison, J. A. Nason, *Environ. Sci. Technol.* **2010**, *45*, 3238.
- [31] L. Tong, Y. Liu, B. D. Dolash, Y. Jung, M. N. Slipchenko, D. E. Bergstrom, J. X. Cheng, *Nat. Nanotechnol.* **2012**, *7*, 56.
- [32] P. Wang, J. Li, P. Wang, C. R. Hu, D. Zhang, M. Sturek, J. X. Cheng, *Angew. Chem.* **2013**, *125*, 13280.
- [33] P. Ramoino, A. Diaspro, M. Fato, C. Usai, in *Molecular Regulation of Endocytosis* (Ed: B. Ceresa), InTech, London, UK **2012**, Ch. 6.
- [34] S. MacLean-Fletcher, T. D. Pollard, *Cell* **1980**, *20*, 329.
- [35] D. Starling, R. Duncan, J. Lloyd, *Cell Biol. Int. Rep.* **1983**, *7*, 593.
- [36] S. E. Gratton, P. A. Ropp, P. D. Pohlhaus, J. C. Luft, V. J. Madden, M. E. Napier, J. M. DeSimone, *Proc. Natl. Acad. Sci. USA* **2008**, *105*, 11613.
- [37] C. Foerg, U. Ziegler, J. Fernandez-Carneado, E. Giralt, R. Rennert, A. G. Beck-Sickingler, H. P. Merkle, *Biochemistry* **2005**, *44*, 72.
- [38] P. van Kerkhof, M. Sachse, J. Klumperman, G. J. Strous, *J. Biol. Chem.* **2001**, *276*, 3778.
- [39] S. K. Rodal, G. Skretting, Ø. Garred, F. Vilhardt, B. Van Deurs, K. Sandvig, *Mol. Biol. Cell* **1999**, *10*, 961.
- [40] L. Pelkmans, D. Püntener, A. Helenius, *Science* **2002**, *296*, 535.
- [41] W. G. Sunda, S. A. Huntsman, *Environ. Sci. Technol.* **1998**, *32*, 2961.
- [42] D. Kühnel, W. Busch, T. Meißner, A. Springer, A. Potthoff, V. Richter, M. Gelinsky, S. Scholz, K. Schirmer, *Aquat. Toxicol.* **2009**, *93*, 91.
- [43] T. Tong, C. M. Wilke, J. Wu, C. T. T. Binh, J. J. Kelly, J. F. Gaillard, K. A. Gray, *Environ. Sci. Technol.* **2015**, *49*, 8113.
- [44] A. J. Miao, K. A. Schwehr, C. Xu, S. J. Zhang, Z. Luo, A. Quigg, P. H. Santschi, *Environ. Pollut.* **2009**, *157*, 3034.
- [45] S. Dryl, *J. Protozool.* **1959**, *6*, 25.
- [46] J. Jaumot, R. Gargallo, A. de Juan, R. Tauler, *Chemom. Intell. Lab. Syst.* **2005**, *76*, 101.
- [47] J. Jaumot, R. Tauler, *Chemom. Intell. Lab. Syst.* **2010**, *103*, 96.
- [48] W. W. Yang, A. J. Miao, L. Y. Yang, *PLoS One* **2012**, *7*, e32300.
- [49] Y. Wang, A. J. Miao, J. Luo, Z. B. Wei, J. J. Zhu, L. Y. Yang, *Environ. Sci. Technol.* **2013**, *47*, 10601.